Atmos. Chem. Phys. Discuss., 5, 9291–9324, 2005
www.atmos-chem-phys.org/acpd/5/9291/
SRef-ID: 1680-7375/acpd/2005-5-9291
European Geosciences Union

Atmospheric Chemistry and Physics Discussions

A computationally efficient inorganic atmospheric aerosol phase equilibrium model (UHAERO)

N. R. Amundson[1], A. Caboussat[1], J. W. He[1], A. V. Martynenko[1], V. B. Savarin[2], J. H. Seinfeld[3], and K. Y. Yoo[4]

[1]Department of Mathematics, University of Houston, Houston, USA
[2]Ecole Nationale Supérieure de Techniques Avancées, Paris, France
[3]Departments of Chemical Engineering and Environmental Science and Engineering, California Institute of Technology, Pasadena, USA
[4]Department of Chemical Engineering, Seoul National University of Technology, Seoul, Korea

Received: 17 August 2005 – Accepted: 13 September 2005 – Published: 28 September 2005

Correspondence to: J. H. Seinfeld (seinfeld@caltech.edu)

Abstract

A variety of thermodynamic models have been developed to predict inorganic gas-aerosol equilibrium. To achieve computational efficiency a number of the models rely on a priori specification of the phases present in certain relative humidity regimes. Presented here is a new computational model, named UHAERO, that is both efficient and rigorously computes phase behavior without any a priori specification. The computational implementation is based on minimization of the Gibbs free energy using a primal-dual method, coupled to a Newton iteration. The mathematical details of the solution are given elsewhere. The model also computes deliquescence and crystallization behavior without any a priori specification of the relative humidities of deliquescence or crystallization. Detailed phase diagrams of the sulfate/nitrate/ammonium/water system are presented as a function of relative humidity at 298.15 K over the complete space of composition.

1 Introduction

The inorganic constituents of atmospheric particles typically consist of electrolytes of ammonium, sodium, calcium, sulfate, nitrate, chloride, carbonate, etc. The phase state of such a mixture at a given temperature and relative humidity will tend to thermodynamic equilibrium with the gas phase. A variety of thermodynamic models have been developed to predict inorganic gas-aerosol equilibrium (Table 1; see also Zhang et al., 2000). The models can be distinguished based on two general features: (1) the method of computing activity coefficients of the aerosol-phase species; and (2) the numerical technique that is used to determine the equilibrium state. Obtaining the equilibrium composition of the aerosol is challenging because multiple liquid and/or solid phases can exist, depending on the chemical composition, ambient relative humidity (RH), and temperature.

One may calculate the composition of the aerosol either by solving the set of non-

linear algebraic equations derived from mass balances and chemical equilibrium or by performing a direct minimization of the Gibbs free energy. Direct minimization of the Gibbs free energy has tended to be computationally demanding, making its use in large-scale atmospheric models unattractive, since the thermodynamic model must, in principle, be implemented in each grid cell at each time step. The most challenging aspect of the numerical determination of the equilibrium is prediction of the partitioning of the inorganic components between aqueous and solid phases in the aerosol. For computational efficiency, a number of the current methods (see Table 1) rely on a priori specification of the presence of phases at a certain relative humidity and overall composition; two models that fall into this category are SCAPE2 and ISORROPIA, both of which employ divided RH and composition domains in which only certain equilibria are assumed to hold. While these assumptions greatly facilitate numerical determination of the equilibrium, they lead to approximations in the phase diagram of the system that may be undesirable (Ansari and Pandis, 1999). What is ultimately needed is an efficient computational model for the equilibrium partitioning of aerosol components between aqueous and solid phases that does not rely on a priori knowledge of the presence of certain phases at a given relative humidity and overall composition.

The physical state of the atmospheric aerosol phase depends on the RH history of the particle. As RH increases from a value at which the particles are dry, crystalline particles spontaneously take up water at the deliquescence RH (DRH) transforming into aqueous droplets containing dissolved ions; as RH decreases from a value above the DRH, aqueous particles do not crystallize (effloresce) until the crystallization RH (CRH) is reached. Between the DRH and the CRH, particles may be either crystalline or aqueous, depending on their RH history. The upper and lower branches of the particle diameter versus RH behavior constitute a hysteresis loop, in which crystalline particles below the DRH follow the lower ascending branch and aqueous particles above the CRH follow the upper descending branch. Current aerosol thermodynamic models account for the deliquescence and efflorescence hysteresis based on a priori knowledge of the presence of solid phases at a certain relative humidity and overall

composition. They either assume crystallization of a solid in a multicomponent solution once the RH drops below the DRH of the solid salt, or neglect solidification altogether. What is needed is a model that predicts both deliquescence and crystallization based purely upon the thermodynamics.

The goal of this paper is to present the results of application of a new inorganic gas-aerosol equilibrium model (UHAERO) that is based on a computationally efficient minimization of the Gibbs free energy, and in which no a priori assumptions are made about the phases present at any particular relative humidity and temperature. Also included in the model is a formulation based on classical theory of nucleation kinetics that simulates the transformation from a metastable phase into a thermodynamically more favorable phase. This physically consistent theory predicts explicitly the physical state of the particle and the deliquescence and efflorescence hysteresis. The model is capable of representing the phase transition and state of atmospheric aerosols over the full range of relative humidity regimes.

The next section summarizes the minimization problem; its mathematical foundation and computational implementation are presented elsewhere (Amundson et al., 2005,?). The third section discusses the determination of phase transitions, such as deliquescence and crystallization. The remainder of the paper is devoted to computation of aerosol phase equilibria in the sulfate/nitrate/ammonium system.

2 Determination of equilibrium

The multicomponent chemical equilibrium for a closed gas-aerosol system at constant temperature and pressure and a specified elemental abundance is the solution to the following problem arising from the minimization of the Gibbs free energy, G,

$$\text{Min} \quad G(\boldsymbol{n}_l, \boldsymbol{n}_g, \boldsymbol{n}_s) = \boldsymbol{n}_g^T \boldsymbol{\mu}_g + \boldsymbol{n}_l^T \boldsymbol{\mu}_l + \boldsymbol{n}_s^T \boldsymbol{\mu}_s, \tag{1}$$

subject to $\boldsymbol{n}_g > \boldsymbol{0}$, $\boldsymbol{n}_l > \boldsymbol{0}$, $\boldsymbol{n}_s \geq \boldsymbol{0}$, and

$$\boldsymbol{A}_g \boldsymbol{n}_g + \boldsymbol{A}_l \boldsymbol{n}_l + \boldsymbol{A}_s \boldsymbol{n}_s = \boldsymbol{b}, \tag{2}$$

where $\boldsymbol{n}_g$, $\boldsymbol{n}_l$, $\boldsymbol{n}_s$ are the concentration vectors in gas, liquid, and solid phases, respectively, $\boldsymbol{\mu}_g$, $\boldsymbol{\mu}_l$, $\boldsymbol{\mu}_s$ are the corresponding chemical potential vectors, $\boldsymbol{A}_g$, $\boldsymbol{A}_l$, $\boldsymbol{A}_s$ are the component-based formula matrices, and $\boldsymbol{b}$ is the component-based feed vector. Condition (2) expresses the fact, for example, that in calculating the partition of sulfate between aqueous and solid phases the total sulfate concentration is conserved, while maintaining a charge balance in solution.

The chemical potential vectors are given by

$$\boldsymbol{\mu}_g = \boldsymbol{\mu}_g^0 + RT \ln \boldsymbol{a}_g, \tag{3}$$

$$\boldsymbol{\mu}_l = \boldsymbol{\mu}_l^0 + RT \ln \boldsymbol{a}_l, \tag{4}$$

$$\boldsymbol{\mu}_s = \boldsymbol{\mu}_s^0, \tag{5}$$

where R is the universal gas constant, T is the system temperature, $\boldsymbol{\mu}_g^0$ and $\boldsymbol{\mu}_l^0$ are the standard chemical potentials of gas and liquid species, respectively, and $\boldsymbol{a}_g$ and $\boldsymbol{a}_l$ are the activity vectors of the gas and liquid species. For ionic components the elements of the activity vector $a_i = \gamma_i m_i$, where γ_i and m_i are the activity coefficient and molality (mol kg^{-1} water), respectively, of component i. The water activity is denoted by a_w. Equations (1)–(5) represent a constrained nonlinear minimization problem.

Water exists in the atmosphere in an amount on the order of g m^{-3} of air while in the aerosol phase at less than 1 mg m^{-3} of air. As a result, the transport of water to and from the aerosol phase does not affect the ambient partial pressure of water in the atmosphere, which is controlled by larger scale meteorological factors. Thus the equilibrium of water between the gas and aerosol phases is defined by $a_w = RH$, where RH is the relative humidity in the atmosphere, expressed as a fraction (Seinfeld and Pandis, 1998).

The key parameters in the equilibrium calculation are the activity coefficients. For aqueous inorganic electrolyte solutions, the Pitzer molality-based model (Pitzer, 1973, 1975; Pitzer and Mayorga, 1973) had been widely used, but it is restricted to high RH regions where solute molalities are low. These concentration restrictions were relaxed with the Pitzer, Simonson, Clegg (PSC) mole fraction-based model (Clegg and

Pitzer, 1992; Clegg et al., 1992). On a mole fraction scale, the activity of component i is expressed as $a_i = f_i\, x_i$, where f_i is the mole fraction-based activity coefficient, and x_i is the mole fraction of species i. The molality- and mole fraction-based activity coefficients are related by $f_i x_w = \gamma_i$. A number of methods exist for calculating the water activity a_w. The most widely used is the ZSR mixing rule (Stokes and Robinson, 1966; Clegg et al., 2003), in which only data on binary solute/water solutions are needed to predict the water content of a multicomponent mixture. A more accurate determination of the water content can be obtained using the solvent activity model of Clegg et al. (1998a,b), which includes interactions between solutes, in addition to those between the solutes and water; in this case, the water activity is calculated from $a_w = f_w x_w$.

The numerical algorithm for thermodynamic equilibrium problems related to modeling of atmospheric inorganic aerosols has been implemented in UHAERO as module 1 (inorganic thermo) and incorporated together with two mole fraction based multicomponent activity coefficient models, namely the PSC model and the Extended UNIQUAC (ExUNIQUAC) model (Thomsen and Rasmussen, 1999). The PSC model has been incorporated in the Aerosol Inorganic Model (AIM). The AIM thermodynamic models are considered as the most comprehensive and accurate over the entire range of compositions and relative humidities. To assess the computational performance, UHAERO module 1 using PSC (UHAERO-PSC) will be benchmarked against predictions obtained with AIM. The phase state and chemical composition of ammonium/sulfate/nitrate aerosols at thermodynamic equilibrium will be investigated via the reconstruction of comprehensive phase-diagrams. UHAERO-PSC can be run in two modes: (1) the water content in the system is specified; (2) the system is equilibrated to a fixed relative humidity (RH). In case (2), the aerosol water content is directly computed from the minimization process, i.e., without using an empirical relationship such as the ZSR equation. The water activity is predicted using PSC in both cases. Also, in both cases, the equilibration of trace gases between the vapor and condensed phases can be enabled or disabled as required, as can the formation of solids, which allows the properties of liquid aerosols supersaturated with respect to solid phases to

be investigated.

The numerical minimization technique of UHAERO is based on a primal-dual active-set algorithm, which is described in detail elsewhere (Amundson et al., 2005,?). In short, the algorithm applies Newton's method to the perturbed Karush-Kuhn-Tucker (KKT) system of equations arising from the minimization of G at each step to find the next primal-dual approximation of the solution. The active set method adds a solid salt when the components reach saturation and deletes a solid phase from the active set when its concentration violates the non-negativity constraint. Phase stability criteria are incorporated into the algorithm to ensure that it converges to a stable equilibrium rather than to any other first-order optimality point, such as a maximum, a saddle point, or an unstable local minimum.

3 Computation of the crystallization of metastable solutions

Transformation from a metastable phase, such as a supersaturated aqueous solution, to a thermodynamically more favorable phase, such as a crystal salt, is initiated by the nucleation and growth of a germ of the new phase. It is reasonable to assume that the overall time over which crystallization occurs is controlled by the time required for nucleation of a single germ, and that the subsequent crystal growth is rapid. The energy required for the formation of a germ of volume V_{germ} and surface area A_{germ} is the difference in the energy cost of creating the two-dimensional interface with the surrounding aqueous medium and the energy released from the three-dimensional association of the germ:

$$\Delta G_{\text{germ}} = -\Delta\mu_s \rho^0_{\text{germ}} V_{\text{germ}} + \sigma_{\text{germ}} A_{\text{germ}}. \tag{6}$$

where ρ^0_{germ} is the molecular density of the germ and σ_{germ} is its surface tension. The free energy barrier ΔG_{crit} that must be surmounted to form a nucleus of critical size is

that at the maximum of ΔG_{germ}; we have

$$\Delta G_{\text{crit}} = \frac{16\pi}{3} c_{\text{geom}} \frac{\sigma^3_{\text{germ}}}{\left(\rho^0_{\text{germ}} RT \ln S\right)^2}, \tag{7}$$

where S (>1) is the saturation ratio of the aqueous phase, which is supersaturated with respect to the salt that forms a nucleus. Thus, ΔG_{crit} is the energy required for the formation of a critical nucleus for which the energy released from its formation exceeds the energy cost of creating the interface with the medium. In Eq. (7), the constant factor c_{geom} is a geometrical parameter defined as

$$c_{\text{geom}} = \frac{1}{36\pi} \frac{A^3_{\text{germ}}}{V^2_{\text{germ}}}. \tag{8}$$

In general, $c_{\text{geom}} \geq 1$, where $c_{\text{geom}}=1$ holds for a spherical nucleus. For a cubic nucleus, $c_{\text{geom}} \geq \frac{6}{\pi} \approx 1.909$. For most salts of interest here, $c_{\text{geom}} \approx 2$. In Table 3 of Cohen et al. (1987), $c_{\text{geom,NaCl}} = \frac{6}{\pi}$ and $c_{\text{geom,}(NH_4)_2SO_4} = 2.072$; no data are available for other crystals. In the present calculation, we employ the approximation $c_{\text{geom,}(NH_4)_3H(SO_4)_2} = c_{\text{geom,}(NH_4)_2SO_4}$. The molecular density of the germ ρ^0_{germ} can be obtained via $\rho^0_{\text{germ}} := \frac{1}{v^0_{\text{germ}}}$, where v^0_{germ} is the molecular volume. In Table 1 of Tang and Munkelwitz (1994) $v^0_{\text{germ}} = 85.307$ for $(NH_4)_2SO_4$ and 148.99 for $(NH_4)_3H(SO_4)_2$; no data are available for other crystals.

According to classical nucleation theory, the nucleation rate J_{nucl} ($\text{cm}^{-3}\,\text{s}^{-1}$), describing the number of nuclei (i.e., a critical germ) formed per volume per time, is given by:

$$J_{\text{nucl}} = J_0 \exp\left(\frac{-\Delta G_{\text{crit}}}{kT}\right), \tag{9}$$

where k is the Boltzmann constant, and J_0 ($\text{cm}^{-3}\,\text{s}^{-1}$) is a pre-exponential factor that is related to the efficiency with which collisions between supernatant ions and the crystal

interface produce crystal growth. J_0 usually is approximated by $J_0 \approx n\frac{kT}{h}$, where N is the molecular concentration in the liquid phase and h is Planck's constant. J_0 has a value of order 10^{24}-10^{36}, and we choose $J_0=10^{30}$ here. For salt nucleation from an aqueous supersaturated droplet, the nucleation rate J_{nucl} depends on the mole fraction composition of the aqueous particle and, consequently, ambient relative humidity when water activity is maintained in equilibrium with the gas-phase. Nucleation is a stochastic process, that can be approximated by the Poisson distribution. After a time, t, the probability of an individual particle having produced a critical nucleus is given by $P_{\mathrm{nucl}}(t)=1-\exp(-J_{\mathrm{nucl}}\, V_p\, t)$, where V_p (cm^3) is the particle volume. This probability also describes complete crystallization when crystal growth is rapid compared to the nucleation time. The expectation time τ_{nucl} after which a particle of volume V_p forms a single nucleus is given by $\tau_{\mathrm{nucl}}=\frac{1}{J_{\mathrm{nucl}}\, V_p}$.

In order to apply the classical nucleation theory (CNT) in the computation of crystallization of salts on the metastable branch of the hysteresis curve, one needs surface tension data for the supersaturated aqueous salts solutions. Although a number of methods for calculating surface tension of dilute aqueous solutions of single electrolytes exist, there are few theoretical models available for the surface tension of aqueous solutions of highly concentrated and mixed electrolytes (Chen, 1994; Li et al., 1999; Li and Lu, 2001; Hu and Lee, 2004). Topping et al. (2005) present a summary of models for the surface tension of aqueous electrolyte solutions. We first calculate the surface tensions for the single-electrolyte aqueous solutions, H_2SO_4 and $(NH_4)_2SO_4$, respectively, to correlate model parameters against the laboratory data reported in Martin et al. (2000) for H_2SO_4/H_2O and HNO_3/H_2O and in Korhonen et al. (1998) for $(NH_4)_2SO_4/H_2O$. No data are available for NH_4NO_3/H_2O. We employ Li and Lu's (Li and Lu, 2001) formula for the surface tension of single electrolyte aqueous solutions,

$$\sigma = \sigma_w - RT\Gamma_{\mathrm{MX}}^{w_0} \ln(1 + K_{\mathrm{MX}} a_{\mathrm{MX}}), \tag{10}$$

where σ_w is the pure water surface tension at the system temperature and a_{MX} is the activity of the electrolyte MX. The two parameters of Eq. (10), $\Gamma_{\mathrm{MX}}^{w_0}$ and K_{MX} are ob-

tained from correlating the surface tension σ against the measurements of Martin et al. (2000) and Korhonen et al. (1998) for MX=H_2SO_4 and MX=$(NH_4)_2SO_4$, respectively. Without introducing any additional parameters or empirical coefficients, the fitted parameters are capable of predicting surface tensions of mixed-electrolyte aqueous solutions. The calculation is based the formula for the surface tension of mixed electrolyte aqueous solutions (Li and Lu, 2001),

$$\sigma = \sigma_w - RT \sum_{i=1}^{n} \Gamma_i^{w_0} \ln(1 + K_i a_i), \tag{11}$$

where, for the binary system $(NH_4)_2SO_4/H_2SO_4$, we have $n=2$, $i \in \{1,2\}=\{(NH_4)_2SO_4, H_2SO_4\}$, and $\Gamma_i^{w_0}$ and K_i are determined from Eq. (10). Note that, for the predicted surface tension of this binary aqueous electrolyte system, the acid and its salt have opposite effects on surface tension as their concentrations increase.

We employ Antonoff's rule to obtain the surface tension of crystalline germs in aqueous electrolyte solutions, σ_{germ} (i.e., between the crystal and the liquid), as the absolute value of the difference between $\sigma_{\mathrm{crystal/air}}$ and $\sigma_{\mathrm{liquid/air}}$; that is

$$\sigma_{\mathrm{germ}} := \sigma_{\mathrm{crystal/liquid}} = |\sigma_{\mathrm{crystal/air}} - \sigma_{\mathrm{liquid/air}}|. \tag{12}$$

In Eq. (12), the surface tension of aqueous electrolyte solutions $\sigma_{\mathrm{liquid/air}}$ can be obtained from Eq. (11), whereas $\sigma_{\mathrm{crystal/air}}$ is a constant for a given crystal and can be determined as a parameter based on one value of σ_{germ}, which, in turn, can be computed from one measurement of the efflorescence RH of the corresponding crystalline salt. Data for the surface tension of salt $(NH_4)_2SO_4$ in the solute mixture of ASR=2 (ASR: ammonium-sulfate-ratio) are reported by Cohen et al. (1987). The measured value $\sigma_{(NH_4)_2SO_4}(\mathrm{ASR}=2)=0.0368\ \mathrm{kg\,s^{-2}}$ is then used to determine the parameter $\sigma_{\mathrm{crystal/air}}$ in Eq. (12) for the calculation of the surface tension of crystalline germs of $(NH_4)_2SO_4$ in aqueous electrolyte solutions of 0<ASR<2. Since there are apparently no laboratory data for the surface tension of the salt $(NH_4)_3H(SO_4)_2$, the parameter $\sigma_{\mathrm{crystal/air}}$ in Eq. (12) for $(NH_4)_3H(SO_4)_2$ is computed from the measured efflorescence RH of

the corresponding crystalline salt in the solute mixture of ASR=1.5, reported by Martin et al. (2003). More precisely, the surface tension of crystalline germs $(NH_4)_3H(SO_4)_2$ in aqueous electrolyte solutions of 0<ASR<2 is determined by adjusting the parameter $\sigma_{crystal/air}$ in Eq. (12) so that its value at ASR=1.5 matches the lower bound of the measured efflorescence RH=22%.

The active-set numerical solution strategy described above has been extended to the computation of crystallization, the details of which are given elsewhere (Amundson et al., 2005). In short, the supersaturated aqueous salts that are expected to crystallize in a given time interval are converted into crystalline components. Then the matrix algebra is updated to reflect the new set of crystal components, and the minimization problem is solved by Newton iteration.

4 Simulation of inorganic phase equilibria and deliquescence/crystallization

The system that is arguably the most important with respect to atmospheric gas-aerosol equilibrium and aerosol state is that of sulfate, nitrate, ammonium, and water. Particles consisting of such species can be fully aqueous, fully crystalline, or consist of liquid-solid mixtures, depending on the relative concentrations of the components, RH, and temperature (Martin, 2000). In the present work we focus on this system and present results of application of UHAERO to the computation of its phase diagrams.

To reconstruct phase diagrams of the five-component system $SO_4^{2-}/NO_3^-/NH_4^+/H^+/H_2O$, we use the X and Y composition coordinates introduced by Potukuchi and Wexler (1995) and define:

$$X = \text{Ammonium Fraction} = \frac{b_{NH_4^+}}{b_{NH_4^+} + b_{H^+}}, \tag{13}$$

$$Y = \text{Sulfate Fraction} = \frac{b_{SO_4^{2-}}}{b_{SO_4^{2-}} + b_{NO_3^-}}, \tag{14}$$

where the system feeds $b_{SO_4^{2-}}$, $b_{NO_3^-}$, $b_{NH_4^+}$, and b_{H^+} are subject to electro-neutrality. It is more convenient to use the feeds in term of $(NH_4)_2SO_4/H_2SO_4/NH_4NO_3/HNO_3/H_2O$ and re-define the X and Y coordinates:

$$X = \frac{2b_{(NH_4)_2SO_4} + b_{NH_4NO_3}}{2b_{(NH_4)_2SO_4} + 2b_{H_2SO_4} + b_{NH_4NO_3} + b_{HNO_3}}, \tag{15}$$

$$Y = \frac{b_{(NH_4)_2SO_4} + b_{H_2SO_4}}{b_{(NH_4)_2SO_4} + b_{H_2SO_4} + b_{NH_4NO_3} + b_{HNO_3}}. \tag{16}$$

Thus, for a fixed (X, Y) coordinate, we can define a non-unique feed composition for the system $(NH_4)_2SO_4/H_2SO_4/NH_4NO_3/HNO_3/H_2O$ as $b_{(NH_4)_2SO_4}=\frac{1}{2}X$, $b_{H_2SO_4}=\frac{Y}{1+Y}-\frac{1}{2}X$, $b_{NH_4NO_3}=\frac{1-Y}{1+Y}$, $b_{HNO_3}=0$, if $X\le\frac{Y}{1+Y}$; otherwise, $b_{(NH_4)_2SO_4}=\frac{Y}{1+Y}$, $b_{H_2SO_4}=0$, $b_{NH_4NO_3}=X-\frac{2Y}{1+Y}$, $b_{HNO_3}=1-X$.

For Case (1) where the water content of the system needs to be specified, we introduce an additional coordinate Z that has values between 0 and 1 and define the water content b_{H_2O} to be $b_{H_2O}=\frac{Y}{1+Y}\frac{Z}{1-Z}$. The coordinate Z is actually a water fraction in the sense that it can be interpreted as

$$Z = \frac{(1+Y)b_{H_2O}}{(1+Y)b_{H_2O} + b_{NH_4^+} + b_{H^+}}. \tag{17}$$

To facilitate the computation of the boundaries in phase diagrams, we also introduce the fractions

$$f_{NH_4^+} = \frac{b_{NH_4^+}}{b_{NH_4^+} + b_{H^+} + (1+Y)b_{H_2O}}, \tag{18}$$

$$f_{H^+} = \frac{b_{H^+}}{b_{NH_4^+} + b_{H^+} + (1+Y)b_{H_2O}}, \tag{19}$$

$$f_{H_2O} = 1 - (f_{NH_4^+} + f_{H^+}), \tag{20}$$

which actually are the barycentric coordinates of the unit triangle with vertices (1 + Y)H_2O, NH_4^+ and H^+. For a fixed Y, the (X, Z) coordinate is interchangeable with the fraction coordinate ($f_{NH_4^+}$, f_{H^+}, f_{H_2O}) via $f_{NH_4^+}=X(1-Z)$, $f_{H^+}=(1-X)(1-Z)$, $f_{H_2O}=Z$, and, conversely, $X=\frac{f_{NH_4^+}}{f_{NH_4^+}+f_{H^+}}$, $Z=1-(f_{NH_4^+}+f_{H^+})$. Therefore, the two dimensional (2-D) phase diagrams for fixed Y values can be generated in three coordinate systems: (X, RH), (X, Z) and (f_{H^+}, $f_{NH_4^+}$), which can be chosen on the basis of computational or graphic convenience.

Figure 1 shows the ammonium/sulfate/nitrate phase diagram at 298.15 K computed with UHAERO. Abscissa X is the cation mole fraction arising from NH_4^+, with the remainder coming from H^+. This can be considered as the degree of neutralization of the particle. Ordinate Y is the anion mole fraction arising from SO_4^{2-}, with the balance being made up of NO^{3-}. The four corners of Fig. 1 thus represent sulfuric acid (top left), ammonium sulfate (top right), ammonium nitrate (bottom right), and nitric acid (bottom left). Coordinate Z is the third dimension, which is relative humidity. Figure 1 is identical to Fig. 1a of Martin et al. (2004), which was computed using the same activity coefficient model as that employed here. Seven possible solid phases exist in this system at 298.15 K; these are labeled as A through G. A denotes ammonium sulfate, $(NH_4)_2SO_4$ (AS); B denotes letovicite, $(NH_4)_3H(SO_4)_2$ (LET); C denotes ammonium bisulfate, NH_4HSO_4 (AHS); D denotes ammonium nitrate, NH_4NO_3 (AN); E denotes the mixed salt, $2NH_4NO_3{\cdot}(NH_4)_2SO_4$ (2AN·AS); F denotes the mixed salt, $3NH_4NO_3{\cdot}(NH_4)_2SO_4$ (3AN·AS); and G denotes the mixed salt of ammonium nitrate and ammonium bisulfate, $NH_4NO_3{\cdot}NH_4HSO_4$ (AN·AHS). Regions outlined by heavy black lines show the first solid that reaches saturation with decreasing RH. The thin labeled solid lines are deliquescence relative humidity contours, and the dotted lines give the aqueous-phase X-Y composition variation with decreasing relative humidity as more solid crystallizes. These so-called liquidus lines were introduced by Potukuchi and Wexler (1995).

Figures 2a, 4a, 6a, 8a and 10a show the computed phase diagrams in the

(X, RH) coordinate, with tracking of the presence of each phase, for the system $(NH_4)_2SO_4/H_2SO_4/NH_4NO_3/HNO_3/H_2O$ at 298.15 K and fixed sulfate fraction $Y=1$, 0.85, 0.5, 0.3 and 0.2, respectively. For each region of space whose boundaries are marked with bold lines, the existing phases at equilibrium are represented. Labels on the contours (—) present the aqueous phase pH values (defined as $pH=-\log_{10} a_{H^+}$) as a function of X and RH. Accordingly, Figs. 2b, 4b, 6b, 8b and 10b show relative particle mass contours (—) as a function of X and RH for the system $(NH_4)_2SO_4/H_2SO_4/NH_4NO_3/HNO_3/H_2O$ at 298.15 K and fixed sulfate fraction $Y=1$, 0.85, 0.5, 0.3 and 0.2, respectively. The relative particle mass, also called particle mass growth factor, is defined as the ratio $\frac{W_p}{W_{dry}}$ of the particle mass W_p at a specific RH and (X,Y) composition with respect to the particle mass W_{dry} of the same (X, Y) composition at the "dry-state". Since $W=W_{dry}+W_{water}$, where W_{water} is the water content in the particle system, by subtracting by 1, the relative particle mass gives the relative water content $\frac{W_{water}}{W_{dry}}$ in the particle system.

To further demonstrate the capability for simulating the deliquescence behavior, Figs. 3, 5, 7, 9 and 11 show deliquescence curves for the system $(NH_4)_2SO_4/H_2SO_4/H_2O$ at 298.15 K for various (X, Y) compositions. These figures correspond to the vertical cuts at the corresponding X-values in Figs. 2 ($Y=1$), 4 ($Y=0.85$), 6 ($Y=0.5$), 8 ($Y=0.3$), and 10 ($Y=0.2$).

Figure 12 depicts the efflorescence RH for the system $(NH_4)_2SO_4/H_2SO_4/H_2O$ at 298.15 K. The activity coefficient calculation is carried out using the ExUNIQUAC based thermodynamic model (Thomsen and Rasmussen, 1999). The labeled solid lines are the efflorescence RH curves that are reconstructed based on the expectation time contours of efflorescence. Labels on the contours (—) present the expectation time (min) of efflorescence in log scale, $\log \tau_{nucl}$, for AS and LET. The dotted line and dashed line are the crystallization RH observations of initial crystal formation and complete crystallization, respectively, reported in Martin et al. (2003), where laboratory data of the crystallization RH of particles at 293 K throughout the entire sulfate-nitrate-

ammonium composition space are expressed as an empirical polynomial.

5 Computational efficiency

The initialization of UHAERO has two modes depending on the circumstance of its application: (a) a so-called cold start, in which no a priori information is available and the system is initialized as an infinitely dilute solution, or (b) a warm-start, in which a convergent solution of a neighbor state is available to initialize the system; this is the case when applying it in conjunction with a 3-D chemical transport model. The computational cost for Case (1) (i.e., the water content is specified) is estimated with the model runs for generating phase diagrams. For the contour plots shown in Fig. 13, a uniform grid with $\frac{1}{2}n(n+1)$ (n=100) points on the unit triangle is used. When the warm start strategy is applied where the model run for the (i,j) point is initialized with the solution of the (i,j-1) point, the elapsed time is 2.32 s (for Y=0.85) on a Linux PC equipped with Intel(R) Pentium(R) 4 CPU 3.06 GHz processor. It requires an average 4.25 Newton iterations per grid point with a stopping criterion for convergence being that the square-root of the residuals does not exceed 10^{-8}. If a cold start is used for generating contours, the average number of Newton iterations required for the convergence is 14.6. The computational cost for Case (2) (RH is fixed) is in the same order as that of Case (1). By using a uniform grid of n^2 points (n=100) on the unit square and applying the same warm-start strategy, the generation of the contour plots in the (X, RH) coordinate as shown in Fig. 4 takes 4.3 s (for Y=0.85), a time that is doubled in comparison with Case (1) due to the doubling of the grid points. The average Newton iterations per grid point is 4.1. The computation times quoted above are those for generation of the entire phase diagram of 10^4 points. If implemented in a 3-D atmospheric model with, say, 50×50×10=25 000 grid cells, then the total computing time needed per time step for the thermodynamic calculation is estimated to be about 10 s. Moreover, this corresponds to a very strict convergence criterion that the square root of the residuals is less than 10^{-8}. The same efficiency is achieved in either mode of

application; there is no need, for example, to iterate on the water content as is required in several other models.

6 Conclusions

Aerosol thermodynamic equilibrium models are a basic component of three-dimensional atmospheric chemical transport models of aerosols. Because these equilibrium models are computationally intensive, those that are currently implemented in 3-D models incorporate a priori specification of phase behavior in order to facilitate computation. Presented here is a new inorganic aerosol thermodynamic computational model that is sufficiently numerically efficient to be included directly in 3-D atmospheric models. The model also includes a first-principles calculation of deliquescence/crystallization behavior based on liquid-solid nucleation theory. Extensive results are presented for the phase behavior in the sulfate/nitrate/ammonium/water system, using the Pitzer-Simonson-Clegg (PSC) activity coefficient model.

Acknowledgements. This work was supported by US Environmental Protection Agency grant X-83234201. The authors thank S. L. Clegg for providing the code for the PSC model based activity coefficient calculation.

References

Amundson, N. R., Caboussat, A., He, J.-W., Seinfeld, J. H., and Yoo, K.-Y.: An optimization problem related to the modeling of atmospheric inorganic aerosols, C. R. Acad. Sci. Paris, Ser. I, 340, 683–686, doi:10.1016/j.crma.2005.01.025, 2005. 9294, 9297

Amundson, N. R., Caboussat, A., He, J.-W., Seinfeld, J. H., and Yoo, K.-Y.: A primal-dual active-set algorithm for chemical equilibrium problems related to modeling of atmospheric inorganic aerosols, J. Optimization Theory Appl., accepted, 2005. 9294, 9297, 9301

Ansari, A. S. and Pandis, S. N.: Prediction of multicomponent inorganic atmospheric aerosol behavior, Atmos. Environ., 33, 745–757, doi:10.1016/S1352-2310(98)00221-0, 1999. 9293, 9311

Bromley, L. A.: Thermodynamic properties of strong electrolytes in aqueous Solutions, AIChE Journal, 19, 313–320, 1973. 9311

Chen, J. P.: Theory of deliquescence and modified kohler curves, J. Atmos. Sci., 51, 3505–3516, 1994. 9299

Clegg, S. L. and Pitzer, K. S.: Thermodynamics of multicomponent, miscible, ionic solutions: generalized equations for symmetrical electrolytes, J. Phys. Chem., 96, 3513–3520, 1992. 9295

Clegg, S. L., Pitzer, K. S., and Brimblecombe, P.: Thermodynamics of multicomponent, miscible, ionic solutions. Mixtures including unsymmetrical electrolytes, J. Phys. Chem., 96, 9470–9479, 1992. 9296, 9311

Clegg, S. L., Brimblecombe, P., and Wexler, A. S.: Thermodynamic Model of the System H^+–NH_4^+–SO_4^{2-}–NO_3^-–H_2O at Tropospheric Temperatures, J. Phys. Chem. A, 102, 2137–2154, 1998a. 9296, 9311

Clegg, S. L., Brimblecombe, P., and Wexler, A. S.: Thermodynamic Model of the System H^+–NH_4^+–Na^+–SO_4^{2-}–NO_3^-–Cl^-–H_2O at 298.15 K, J. Phys. Chem. A, 102, 2155–2171, 1998b. 9296, 9311

Clegg, S. L., Seinfeld, J. H., and Edney, E. O.: Thermodynamic modelling of aqueous aerosols containing electrolytes and dissolved organic compounds. II. An extended Zdanovskii-Stokes-Robinson approach, J. Aerosol Sci., 34, 667–690, doi:10.1016/S0021-8502(03)00019-3, 2003. 9296

Cohen, M. D., Flagan, R. C., and Seinfeld, J. H.: Studies of Concentrated Electrolyte Solutions Using the Electrodynamic Balance. 3. Solute Nucleation, J. Phys. Chem., 91, 4583–4590, 1987. 9298, 9300

Hu, Y. F. and Lee, H.: Prediction of the surface tension of mixed electrolyte solutions based on the equation of Patwardhan and Kumar and the fundamental Butler equations, J. Colloid Interface Sci., 269, 442–448, 2004. 9299

Jacobson, M., Tabazadeh, A., and Turco, R.: Simulating equilibrium within aerosols and nonequilibrium between gases and aerosols, J. Geophys. Res., 101, 9079–9091, 1996. 9311

Jacobson, M. Z.: Studying the effects of calcium and magnesium on size-distributed nitrate and

ammonium with EQUISOLV II, Atmos. Environ., 30, 3635–3649, 1999. 9311

Kim, Y. P. and Seinfeld, J. H.: Atmospheric Gas-Aerosol Equilibrium III. Thermodynamics of Crustal Elements Ca^{2+}, K^+, and Mg^{2+}, Aerosol Sci. Technol., 22, 93–110, 1995. 9311

Kim, Y. P., Seinfeld, J. H., and Saxena, P.: Atmopsheric gas-aerosol equilibrium I. Thermodynamic model, Aerosol Science and Technology, 19, 157–181, 1993a. 9311

Kim, Y. P., Seinfeld, J. H., and Saxena, P.: Atmospheric Gas-Aerosol Equilibrium II. Analysis of Common Approximations and Activity Coefficient Calculation Methods, Aerosol Sci. Technol., 19, 182–198, 1993b. 9311

Korhonen, P., Laaksonen, A., Batris, E., and Viisanen, Y.: Thermodynamics for highly concentrated water – ammonium sulfate solutions, J. Aerosol Sci., 29, S379–S380, 1998. 9299, 9300

Kusik, C. L. and Meissner, H. P.: Electrolyte activity coefficients in inorganic processing, AIChE Symposium Series, 173, 14–20, 1978. 9311

Li, Z. and Lu, B. C.: Surface tension of aqueous electrolyte solutions at high concentrations – representation and prediction, Chem. Eng. Sci., 56, 2879–2888, 2001. 9299, 9300

Li, Z. B., Li, Y. G., and Lu, J. F.: Surface tension model for concentrated electrolyte aqueous solutions by the Pitzer equation, Ind. Eng. Chem. Res., 33, 1133–1139, 1999. 9299

Martin, M., George, G., and Mirabel, P.: Densities and Surface tensions of $H_2SO_4/HNO_3/H_2O$ solution, Geophys. Res. Lett., 27, 197–200, 2000. 9299, 9300

Martin, S. T.: Phase Transitions of Aqueous Atmospheric Particles, Chem. Rev., 100, 3403–3454, doi:10.1021/cr990034t, 2000. 9301

Martin, S. T., Schlenker, J. C., Malinowski, A., Hung, H.-M., and Rudich, Y.: Crystallization of atmospheric sulfate-nitrate-ammonium particles, Geophys. Res. Lett., 30, 2102, doi:10.1029/2003GL017930, 2003. 9301, 9304, 9323

Martin, S. T., Hung, H.-M., Park, R. J., Jacob, D. J., Spurr, R. J. D., Chance, K. V., and Chin, M.: Effects of the physical state of tropospheric ammonium-sulfate-nitrate particles on global aerosol direct radiative forcing, Atmos. Chem. Phys., 4, 183–214, 2004, SRef-ID: 1680-7324/acp/2004-4-183. 9303, 9312

Meng, Z. Y., Seinfeld, J. H., Saxena, P., and Kim, Y. P.: Atmospheric Gas-Aerosol Equilibrium IV. Thermodynamics of Carbonates, Aerosol Sci. Technol., 23, 131–154, 1995. 9311

Nenes, A., Pandis, S. N., and Pilinis, C.: ISORROPIA: A new thermodynamic equilibrium model for multiphase multicomponent inorganic aerosols, Aquatic Geochemistry, 4, 123–152, 1998.

Pitzer, K. S.: Thermodynamics of electrolytes 1. Theoretical basis and general equations, J. Phys. Chem., 77, 268–277, 1973. 9311 9295

Pitzer, K. S.: Thermodynamics of electrolytes 5. Effects of higher-order electrostatic terms, J. Solution Chem., 4, 249–265, 1975. 9295

Pitzer, K. S. and Mayorga, G.: Thermodynamics of electrolytes, 2. Activity and osmotic coefficients for strong electrolytes with one or both ions univalent, J. Phys. Chem., 77, 2300–2308, 1973. 9295, 9311

Pitzer, K. S. and Simonson, J. M.: Thermodynamics of Multicomponent, Miscible, Ionic Systems: Theory and Equations, J. Phys. Chem., 90, 3005–3009, 1986. 9311

Potukuchi, S. and Wexler, A. S.: Identifying solid-aqueous-phase transitions in atmospheric aerosols. II. Acidic solutions, Atmos. Environ., 29, 3357–3364, doi:10.1016/1352-2310(95)00212-H, 1995. 9301, 9303, 9312

Seinfeld, J. H. and Pandis, S. N.: Atmospheric Chemistry and Physics: From Air Pollution to Climate Change, Wiley, New York, 1998. 9295

Stokes, R. H. and Robinson, R. A.: Interactions in aqueous nonelectrolyte solutions, I. Solute-solvent equilibria, J. Phys. Chem., 70, 2126–2131, 1966. 9296, 9311

Tang, I. N. and Munkelwitz, H. R.: Water activities, densities, and refractive indices of aqueous sulfates and sodium nitrate droplets of atmospheric importance, J. Geophys. Res., 99, 18 801–18 808, 1994. 9298

Thomsen, K. and Rasmussen, P.: Modeling of vapor-liquid-solid equilibrium in gas-aqueous electrolyte systems, Chem. Eng. Sci., 54, 1787–1802, 1999. 9296, 9304, 9311

Topping, D. O., McFiggans, G. B., and Coe, H.: A curved multi-component aerosol hygroscopicity model framework: Part 1 – Inorganic compounds, Atmos. Chem. Phys., 5, 1205–1222, 2005,
SRef-ID: 1680-7324/acp/2005-5-1205. 9299, 9311

Wexler, A. S. and Clegg, S. L.: Atmospheric aerosol models for systems including the ions H^+, NH_4^+, Na^+, SO_4^{2-}, NO_3^-, Cl^-, Br^-, and H_2O, J. Geophys. Res., 107, 4207, doi:10.1029/2001JD000451, 2002. 9311

Zaveri, R. A., Easter, R. C., and Peters, L. K.: MESA: A computationally efficient multicomponent equilibrium solver for aerosol-phase solid/liquid partitioning, J. Geophys. Res., accepted, 2005a.

Zaveri, R. A., Easter, R. C., and Wexler, A. S.: MTEM: A new method for multicomponent activity coefficients of electrolytes in aqueous atmospheric aerosols, J. Geophys. Res., accepted, 2005b. 9311 9311

Zhang, Y., Seigneur, C., Seinfeld, J. H., Jacobson, M., Clegg, S. L., and Binkowski, F. S.: A comparative review of inorganic aerosol thermodynamic equilibrium modules: similarities, differences, and their likely causes, Atmos. Environ., doi:10.1016/S1352-2310(99)00236-8, 2000. 9292

Table 1. Gas-aerosol equilibrium models[1].

Model name[2]	System addressed	Activity coefficient method[3]	Computational method
SCAPE2	$NH_4^+/Na^+/Ca^{2+}/Mg^+/K^+/NO_3^-/SO_4^{-2}/Cl^-/CO_3^{2-}$	Choice of Bromley, KM, Pitzer @ 298.15 K. ZSR for water content.	Classifies problem into one of several subdomains. Nonlinear equations solved by iterative bisection. Each salt assumed to deliquesce at its own DRH.
ISORROPIA	$NH_4^+/Na^+/NO_3^-/SO_4^{-2}/Cl^-$	Bromle @ 298.15 K. ZSR for water content.	Classifies problem into one of several subdomains. Nonlinear equations solved by iterative bisection. Mixture assumed to deliquesce at RH > lowest DRH of all salts present.
EQUISOLV II	$NH_4^+/Na^+/Ca^{2+}/Mg^+/K^+/NO_3^-/SO_4^{-2}/Cl^-/CO_3^{2-}$	Bromley[4]. ZSR for water content.	Nonlinear equations solved one at a time then iterated to to convergence.
GFEMN	$NH_4^+/Na^+/NO_3^-/SO_4^{-2}/Cl^-$	PSC @ 298.15 K. ZSR for water content.	Iterative Gibbs free energy minimization.
AIM2 (Model III)	$NH_4^+/Na^+/NO_3^-/SO_4^{-2}/Cl^-$	PSC @ 298.15 K. ZSR for water content.	Iterative Gibbs free energy minimization.
MESA	solid-liquid: $NH_4^+/Na^+/Ca^{2+}/NO_3^-/SO_4^{-2}/Cl^-$	Choice of PSC, MTEMd/KM, Bromley @ 298.15 K. ZSR for water content.	Simultaneous iteration of all solid-liquid equilibria using pseudo-transient continuation method.
ADDEM	$NH_4^+/Na^+/NO_3^-/SO_4^{-2}/Cl^-$	PSC. Clegg solvent activity model for water content.	FFSQP (Fast Fortran Sequential Quadratic Programming) to minimize Gibbs free energy.
UHAERO	$NH_4^+/Na^+/NO_3^-/SO_4^{-2}/Cl^-$	Choice of PSC, ExUNIQUAC.	Minimization of Gibbs free Energy (see text).

[1] Table adapted from Zaveri et al. (2005b).

[2] SCAPE2 (Kim et al., 1993a,b; Kim and Seinfeld, 1995; Meng et al., 1995); ISORROPIA (Nenes et al., 1998); EQUISOLV II (Jacobson et al., 1996; Jacobson, 1999); GFEMN (Ansari and Pandis, 1999); AIM2 (Clegg et al., 1998a,b; Wexler and Clegg, 2002); MESA (Zaveri et al., 2005a); ADDEM (Topping et al., 2005)

[3] Bromley (Bromley, 1973); KM (Kusik and Meissner, 1978); Pitzer (Pitzer and Mayorga, 1973); PSC (Pitzer and Simonson, 1986; Clegg et al., 1992, 1998a,b; Wexler and Clegg, 2002); MTEM (Zaveri et al., 2005b); ZSR (Stokes and Robinson, 1966); ExUNIQAC (Thomsen and Rasmussen, 1999)

[4] Binary activity coefficients for the electrolytes in the $NH_4^+/Na^+/NO_3^-/SO_4^{-2}/Cl^-$ system are temperature dependent, while they are fixed at 298.15 K for the $Ca^{2+}/Mg^+/K^+/NO_3^-/SO_4^{-2}/Cl^-/CO_3^{2-}$ system.

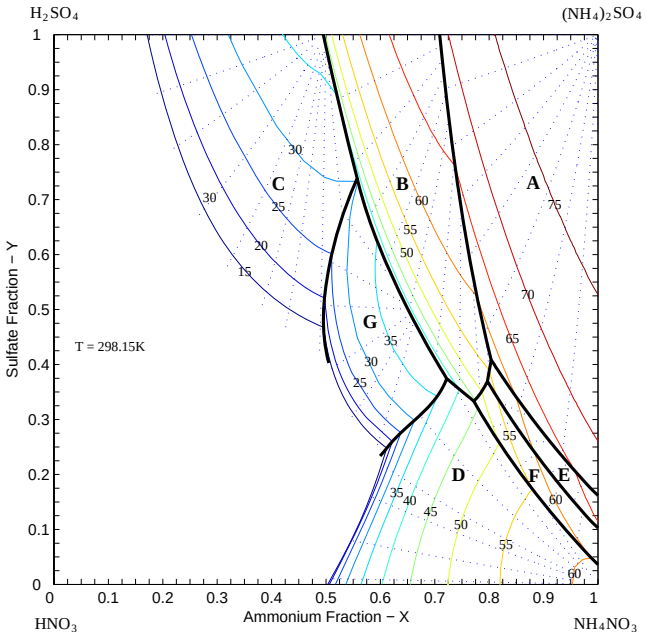

Fig. 1. Water activity contours at saturation (—) for the aqueous solution of $SO_4^{2-}/NO_3^-/NH_4^+/H^+/H_2O$ at 298.15 K. The dotted lines (···) indicate the subsequent aqueous phase (X, Y) composition with decreasing relative humidity as more solid crystallizes. Phase boundaries are marked with bold lines separating different solid phases. All the solid phases are identified and are marked. Labels on the contours present water activities at saturation which represent the deliquescence relative humidity values. This figure corresponds to the contour plot for Fig. 1 in Potukuchi and Wexler (1995) and Fig. 1a in Martin et al. (2004).

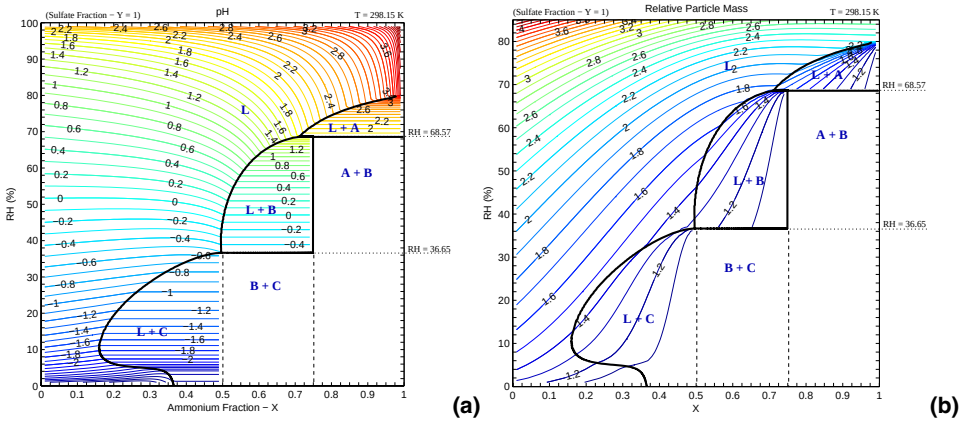

Fig. 2. Reconstruction of the phase diagram for the system $(NH_4)_2SO_4/H_2SO_4/H_2O$ at 298.15 K with tracking of the presence of each phase. For each region of space whose boundaries are marked with bold lines, the existing phases at equilibrium are represented. **(a)** Labels on the contours (—) present the aqueous phase pH values (equal to $-\log_{10} a_{H^+}$). **(b)** Labels on the contours (—) present the relative particle mass.

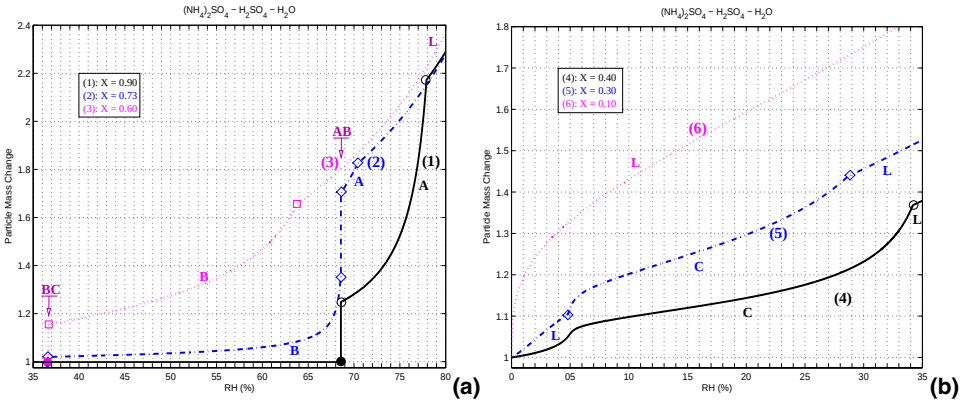

Fig. 3. Deliquescence curves for the system $(NH_4)_2SO_4/H_2SO_4/H_2O$ at 298.15 K. Relative particle mass with changing relative humidity for several values of X. **(a)**: (1) X=0.9, (2) X=0.73, (3) X=0.6. **(b)**: (4) X=0.4, (5) X=0.3, (6) X=0.1. Curves (1) to (6) represent the relative particle mass on the vertical cuts at the corresponding X-values in Fig. 2b.

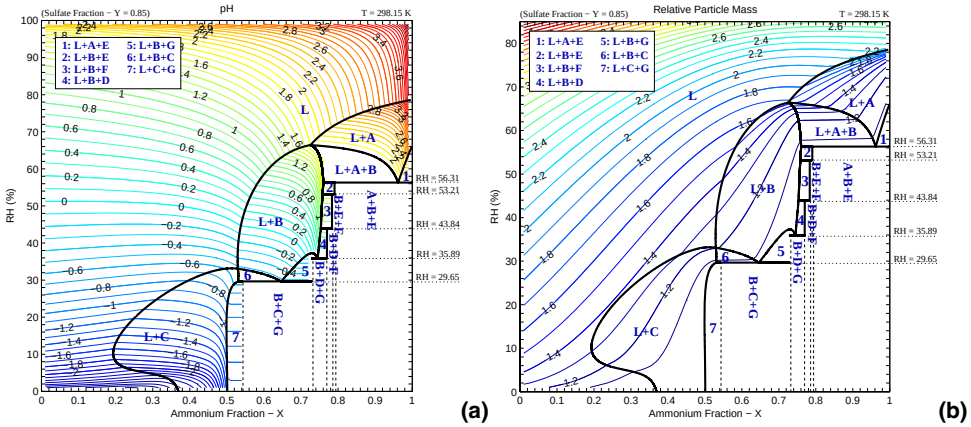

Fig. 4. Reconstruction of the phase diagram for the system $(NH_4)_2SO_4/H_2SO_4/NH_4NO_3/HNO_3/H_2O$ with the sulfate fraction Y=0.85 at 298.15 K with tracking of the presence of each phase. For each region of space whose boundaries are marked with bold lines, the existing phases at equilibrium are represented. **(a)** Labels on the contours (—) present the aqueous phase pH values (equal to $-\log_{10} a_{H^+}$). **(b)** Labels on the contours (—) present the relative particle mass.

9315

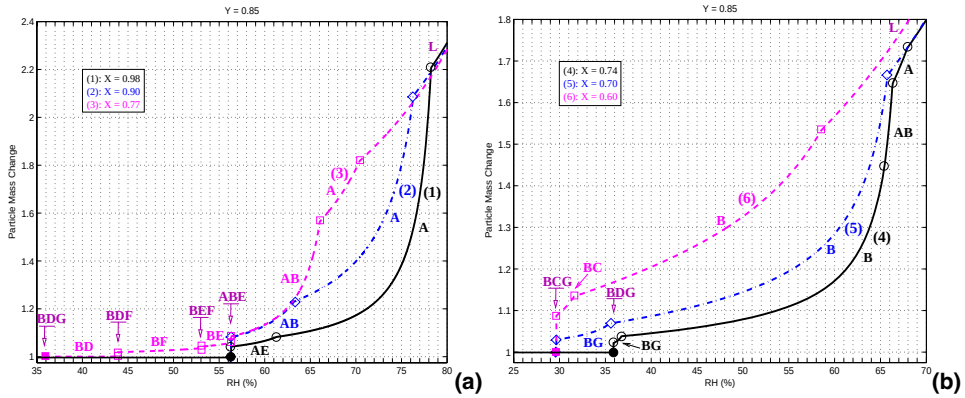

Fig. 5. Deliquescence curves for the system $(NH_4)_2SO_4/H_2SO_4/NH_4NO_3/HNO_3/H_2O$ with the sulfate fraction Y=0.85 at 298.15 K. Relative mass with changing relative humidity for several values of X. **(a)**: (1) X=0.98, (2) X=0.9, (3) X=0.77. **(b)**: (4) X=0.74, (5) X=0.7, (6) X=0.6. Curves (1) to (6) represent the relative particle mass on the vertical cuts at the corresponding X-values in Fig. 4b.

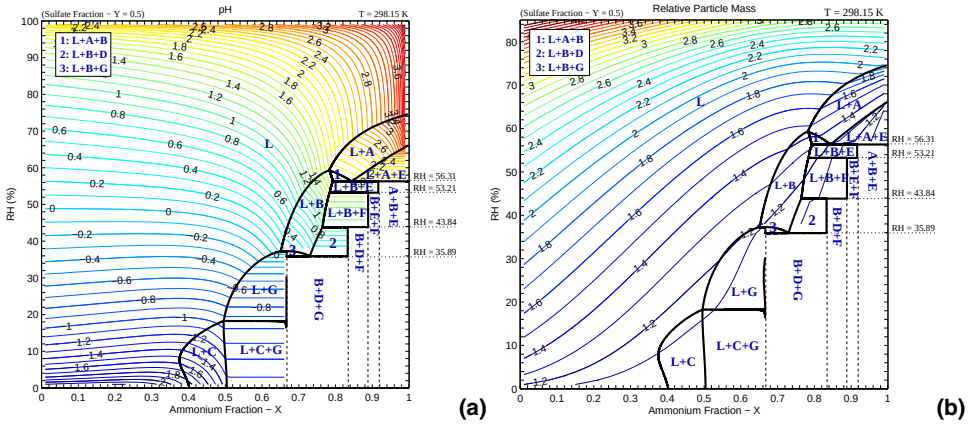

Fig. 6. Reconstruction of the phase diagram for the system $(NH_4)_2SO_4/H_2SO_4/NH_4NO_3/HNO_3/H_2O$ with the sulfate fraction Y=0.5 at 298.15 K with tracking of the presence of each phase. For each region of space whose boundaries are marked with bold lines, the existing phases at equilibrium are represented. **(a)** Labels on the contours (—) present the aqueous phase pH values (equal to $-\log_{10} a_{H^+}$). **(b)** Labels on the contours (—) present the relative particle mass.

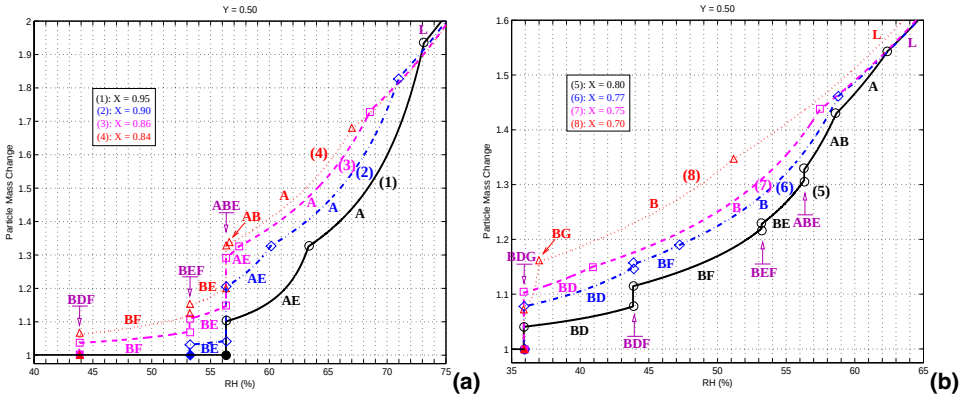

Fig. 7. Deliquescence curves for the system $(NH_4)_2SO_4/H_2SO_4/NH_4NO_3/HNO_3/H_2O$ with the sulfate fraction Y=0.5 at 298.15 K. Relative mass with changing relative humidity for several values of X. **(a)**: (1) X=0.95, (2) X=0.9, (3) X=0.86, (4) X=0.84. **(b)**: (5) X=0.8, (6) X=0.77, (7) X=0.75, (8) X=0.7. Curves (1) to (8) represent the relative particle mass on the vertical cuts at the corresponding X-values in Fig. 6b.

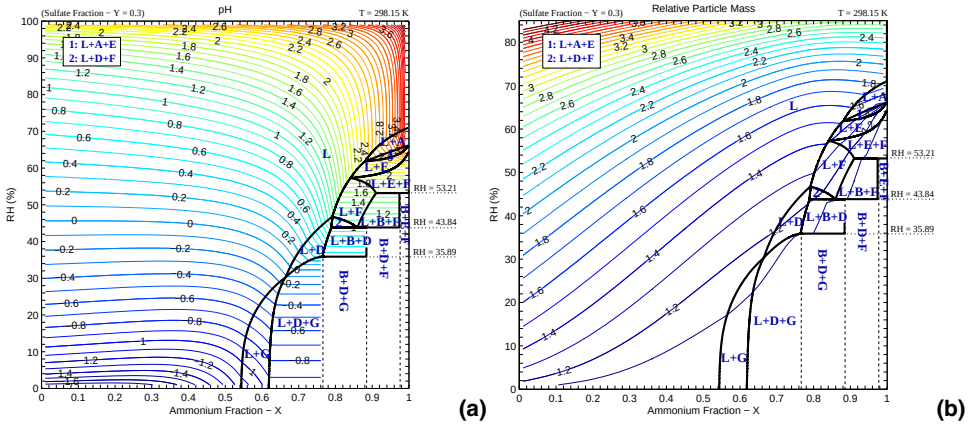

Fig. 8. Reconstruction of the phase diagram for the system $(NH_4)_2SO_4/H_2SO_4/NH_4NO_3/HNO_3/H_2O$ with the sulfate fraction Y=0.3 at 298.15 K with tracking of the presence of each phase. For each region of space whose boundaries are marked with bold lines, the existing phases at equilibrium are represented. **(a)** Labels on the contours (—) present the aqueous phase pH values (equal to $-\log_{10} a_{H^+}$). **(b)** Labels on the contours (—) present the relative particle mass.

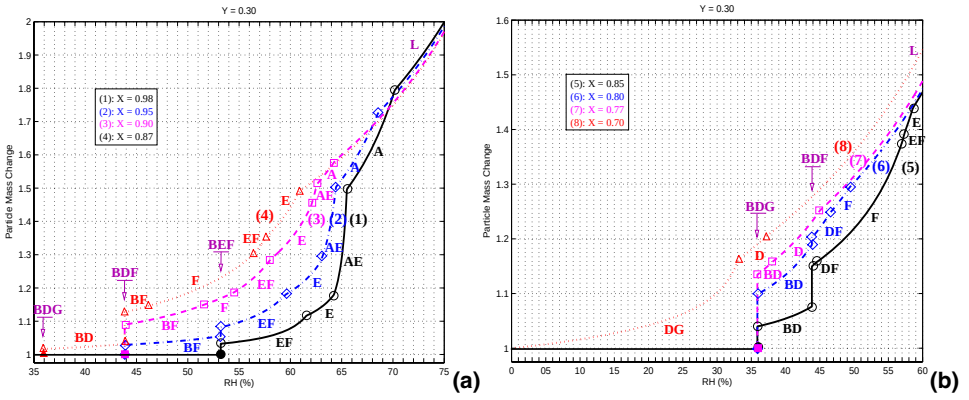

Fig. 9. Deliquescence curves for the system $(NH_4)_2SO_4/H_2SO_4/NH_4NO_3/HNO_3/H_2O$ with the sulfate fraction Y=0.3 at 298.15 K. Relative mass with changing relative humidity for several values of X. **(a)**: (1) X=0.98, (2) X=0.95, (3) X=0.9. **(b)**: (4) X=0.87, (5) X=0.85, (6) X=0.8, (7) X=0.77. Curves (1) to (7) represent the relative particle mass on the vertical cuts at the corresponding X-values in Fig. 8b.

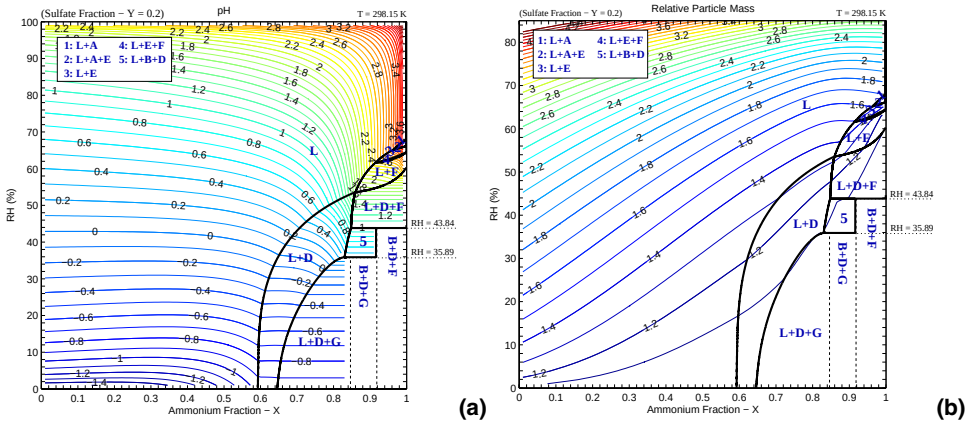

Fig. 10. Reconstruction of the phase diagram for the system $(NH_4)_2SO_4/H_2SO_4/NH_4NO_3/HNO_3/H_2O$ with the sulfate fraction Y=0.2 at 298.15 K with tracking of the presence of each phase. For each region of space whose boundaries are marked with bold lines, the existing phases at equilibrium are represented. **(a)** Labels on the contours (—) present the aqueous phase pH values (equal to $-\log_{10} a_{H^+}$). **(b)** Labels on the contours (—) present the relative particle mass.

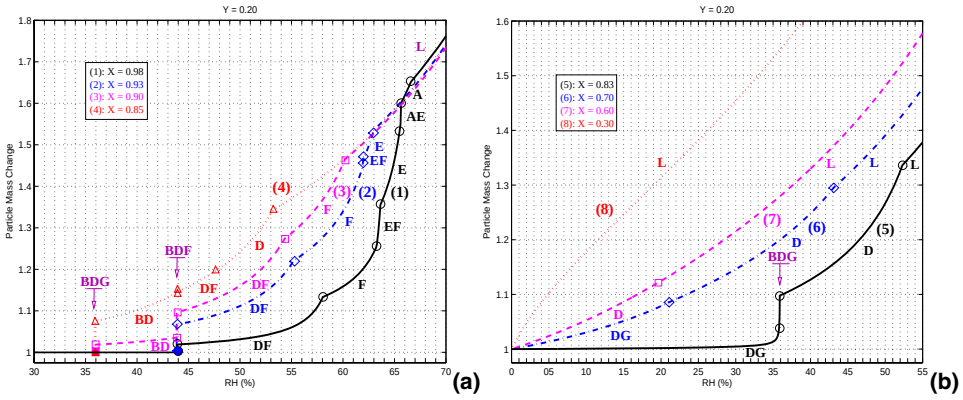

Fig. 11. Deliquescence curves for the system $(NH_4)_2SO_4/H_2SO_4/NH_4NO_3/HNO_3/H_2O$ with the sulfate fraction Y=0.2 at 298.15 K. Relative mass with changing relative humidity for several values of X. **(a)**: (1) X=0.98, (2) X=0.93, (3) X=0.9, (4) X=0.85. **(b)**: (5) X=0.83, (6) X=0.7, (7) X=0.6, (8) X=0.3. Curves (1) to (6) represent the relative particle mass on the vertical cuts at the corresponding X-values in Fig. 10b.

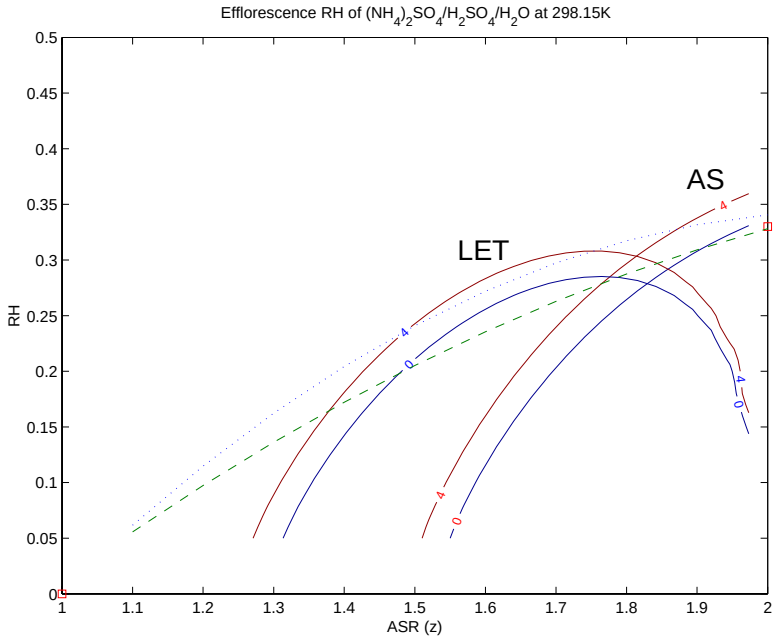

Fig. 12. Efflorescence *RH* for the system $(NH_4)_2SO_4/H_2SO_4/H_2O$ at 298.15 K. Labels on the contours (—) present the expectation time (min) of efflorescence in log scale. The dotted line and dashed line are, respectively, the crystallization *RH* observations at 293 K of initial crystal formation and complete crystallization (Martin et al., 2003).

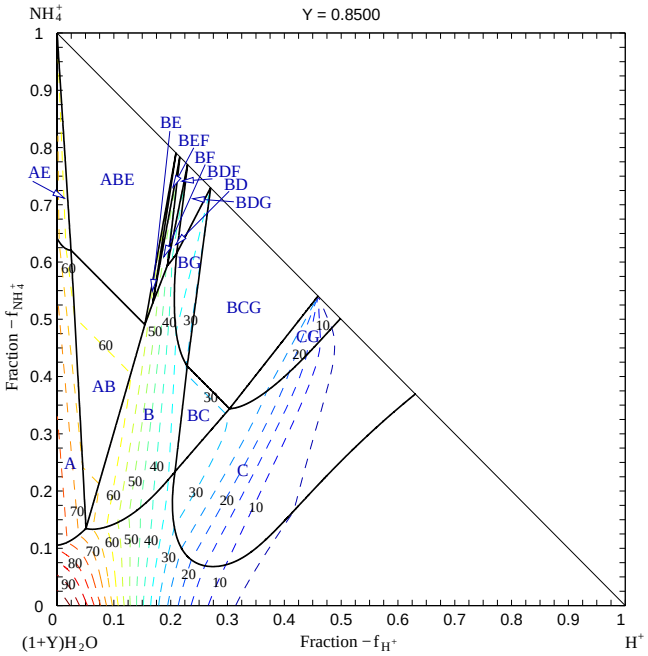

Fig. 13. Reconstruction of the phase diagram for the system $(NH_4)_2SO_4/H_2SO_4/NH_4NO_3/HNO_3/H_2O$ with the sulfate fraction Y=0.85 at 298.15 K in the (f_{H^+}, $f_{NH_4^+}$) coordinate with tracking of the presence of each solid phases. For each region of space whose boundaries are marked with bold lines, the existing solid phases at equilibrium are represented. Labels on the contours (—) present the water activity values as a function of the fractions f_{H^+} and $f_{NH_4^+}$.